ARMA 14-7071

Interaction of multiple fluid-driven fractures with pre-existing discontinuities

Napier, J.A.L.
Department of Mining Engineering, University of Pretoria, South Africa
Peirce, A.P.
Department of Mathematics, University of British Columbia, Canada

This paper was prepared for presentation at the 48th US Rock Mechanics / Geomechanics Symposium held in Minneapolis, MN, USA, 1-4 June 2014.

ABSTRACT: The mechanics of fluid-driven fracture propagation through fracture networks is of central interest in gas and oil extraction procedures. A number of computational strategies have now been developed to simulate these processes although specific understanding of the propagation mechanics in the vicinity of pre-existing discontinuities or faults is still limited. This paper investigates the problem of formulating appropriate fluid branching logic at multiple flow path junctions and the influence of sudden contractions or expansions in the flow path channel width at discontinuity intersections. A plane strain model is assumed. A question of additional interest is the possible existence of a "fluid lag" region between the flow front and the mobilized fracture front. The paper explores some examples of flow propagation and branching through simple joint networks.

1. INTRODUCTION

Extensive theoretical investigations of hydraulic fracture propagation have been carried out following the initial formulation of the problem for the solution of a single fracture driven by internal fluid pressure [1, 2, 3]. In the case of fluid propagation in an impermeable medium, specific considerations relate to the dominant processes governing the coupling between the fluid front and the propagating crack tip (viscous or toughness controlled propagation) and whether a lag may exist between the fluid front and the advancing crack tip [4, 5, 6, 7].

The general numerical analysis of planar fluid-driven fracture propagation requires careful treatment of the crack tip conditions [8, 9, 10]. Additional difficulties arise when the fracture path is non-planar and when flow branching occurs. A number of interesting results have been established for the numerical treatment of the intersection of a propagating fracture with a pre-existing discontinuity [11, 12, 13] indicating that a variety of intricate effects can arise in determining the flow branching conditions and the conditions that determine discontinuity crossing or stepping.

The present paper will present a plane strain formulation for multiple branch flow junctions, including the existence of a fluid lag between the fluid front and the crack tip. It is noted as well that in a pre-existing fracture network, the propagating fluid may initiate and mobilize fractures that are close to fluid-filled segments. Simple numerical simulations are presented to illustrate the behaviour of the model.

2. NETWORK FLOW MODEL

It is assumed that the volumetric fluid flow rate $q(s)$ at position s in a given flow segment is governed by Poiseuille's classical parallel-plate flow velocity averaged over the segment width, $w(s)$, according to the following relationship (see, for example, [15]):

$$q(s) = \frac{-w^3(s)}{12\mu_f}\frac{\partial p}{\partial s}, \qquad (1)$$

where μ_f is the fluid viscosity (Pa.sec) and $\partial p / \partial s$ is the local pressure gradient at position s. Consider the case where multiple flow segments meet at a common junction point as shown in Fig. 1. If p^J is the junction

pressure and if the opening width w_k in each branch k is constant then, from Eq. (1), the flow rate q_k into branch k is given by

$$q_k = \frac{-w_k^3}{12\mu_f}\left[\frac{p^J - p_k}{c_k}\right], \qquad (2)$$

where p_k is the fluid pressure that is assumed to be known at a point within the flow segment, located at a distance c_k from the junction. For no fluid accumulation at the junction, it is required that the sum of the flows into the junction should be zero. Hence, the junction pressure p^J must satisfy the relationship

$$p^J = \frac{\sum_j p_j w_j^3 / c_j}{\sum_j w_j^3 / c_j}. \qquad (3)$$

Substituting Eq. (3) into Eq. (2), gives an expression for each branch flow rate q_k as

$$q_k = \frac{-w_k^3}{12\mu_f c_k}\left[\frac{\sum_{j\neq k}(p_j - p_k) w_j^3 / c_j}{\sum_j w_j^3 / c_j}\right]. \qquad (4)$$

In the particular case where there are $N = 2$ branches,

$$q_1 = -q_2 = \frac{w_1^3 w_2^3 (p_1 - p_2)}{12\mu_f (c_2 w_1^3 + c_1 w_2^3)}. \qquad (5)$$

If $c_1 = c_2$ then Eq. (5) represents the flux obtained by taking the harmonic mean of the cubes of the adjacent widths. It should also be noted that if an estimate of the flow rate through the junction with two branches is made using the average value of the adjacent flow widths, $\overline{w} = (w_1 + w_2)/2$, then

$$\overline{q}_1 = \frac{(w_1 + w_2)^3 (p_1 - p_2)}{192\mu_f c_1}, \qquad (6)$$

provided $c_1 = c_2$. Consequently, defining the width ratio $\rho = w_2 / w_1$, it can be seen that

$$\frac{\overline{q}_1}{q_1} = \frac{(1+\rho)^3 (1+\rho^3)}{16\rho^3}, \qquad (7)$$

and equality between the expressions for q_1 and $\overline{q}_1$ occurs only if $w_1 = w_2$ and $\rho = 1$. The flow rate estimates at all junctions are evaluated using Eq. (4) to allow the uniform treatment of multiple junctions. This is considered to be important as well in the special case where a "kinked" flow path occurs where it is evident that the flow width can be expected to alter discontinuously on each side of the junction.

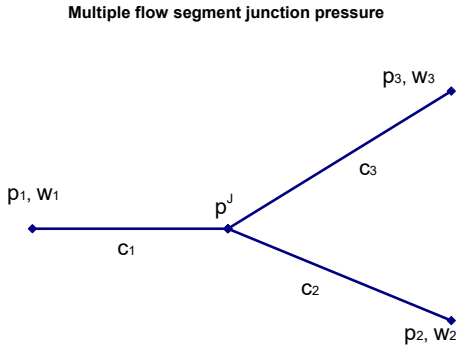

Fig. 1. Schematic depiction of multiple flow segment junction pressure and adjacent flow branch width and pressure values.

3. FRACTURE NETWORK SOLUTION

The fracture segments in a two-dimensional plane strain fracture network are assumed to be represented by a set of straight-line displacement discontinuity boundary elements. Each element has one or more internal collocation points where pressure or traction boundary conditions are required to be satisfied. It is convenient to consider each collocation point to be associated with a specific covering segment having assigned start and end points S_1 and S_2 located at distances c_1 and c_2 from the internal collocation point respectively as indicated in Fig. 2. In general, one or more "external" segment branches may be connected to the segment end points.

The collocation points are distinguished as being non-flow fracture segments or as flow segments. The boundary conditions in the non-flow fracture segments are chosen to satisfy a zero traction condition in open cracks or to obey a defined frictional shear resistance that governs the slip extent across the closed crack surfaces.

Alternatively, if a given collocation point is covered by a fluid-filled segment then the rate of change of the average segment flow width w is determined by the flow volume balance relationship

$$(c_1 + c_2)\frac{\partial w}{\partial t} = \Delta q + Q_0, \qquad (8)$$

where $\Delta q = q_{in} - q_{out}$ represents the difference between the flow rate, q_{in}, into the segment at end point S_1 and

the flow rate, q_{out}, out of the segment at end point S_2. Q_0 is the rate of flow of fluid that is injected into the segment if the collocation point is defined to be a flow source point. Eq. (8) is approximated using an implicit backward difference formula of the form

$$(c_1 + c_2)\left[\frac{w - w^p}{\Delta t}\right] = \Delta q + Q_0 , \qquad (9)$$

where w, Δq and Q_0 are the flow width, flow rate difference and injection rate at the current time t. w^p is the flow width in the previous time step, $t - \Delta t$, with time step interval Δt.

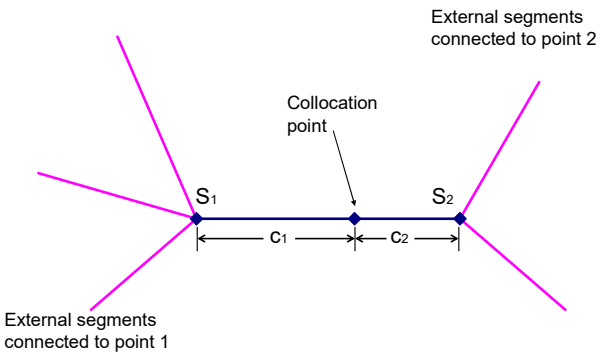

Fig. 2. Layout of a fracture network segment, located between points S_1 and S_2, covering an internal displacement discontinuity collocation point. One or more external segment branches may be connected to each end of the covering segment.

The entire fracture network is solved iteratively within each time step, Δt, to determine the local equilibrium traction and displacement discontinuity vector components at each collocation point. The tractions induced at each collocation point by the entire assembly of displacement discontinuity elements are determined by the appropriate displacement discontinuity influence function expressions [16, 17]. In solving the flow balance relationship Eq. (9) iteratively, it is important to note that the influence relationships imply a connection between the crack opening width w and the fluid pressure p at each collocation point. This may be expressed in the form

$$p = K_n w - E_n , \qquad (10)$$

where K_n represents the crack-normal displacement discontinuity self-effect stiffness and E_n is the overall sum of the crack-normal stress component influence values from all elements "external" to the considered collocation point, plus the crack-normal field stress component. K_n depends on the element length and on the elastic material constants and remains constant for all iterative cycles but E_n varies from cycle to cycle as the solution converges. It can be seen that Eq. (1), Eq. (9) and Eq. (10) imply that the flow rate difference Δq will itself depend on the local value of the width w. Using Equations (2), (3), (4) and (10), the flow rate into the flow segment end S_1, shown in Fig. 2, can be expressed as the following explicit function of w.

$$q_{in}(w) = \frac{w^3}{12\mu_f}\left[\frac{\hat{p}_1 - \hat{w}_1(K_n w - E_n)}{c_1 \hat{w}_1 + w^3}\right], \qquad (11)$$

where,

$$\hat{p}_1 = \sum_{J_1^e} (w_k^e)^3 \, p_k^e / c_k^e , \qquad (12)$$

$$\hat{w}_1 = \sum_{J_1^e} (w_k^e)^3 / c_k^e , \qquad (13)$$

and where the sums are over the set of external flow segments J_1^e that are connected to the edge point S_1 as shown in Fig. 2. The distance between the nearest collocation point in external flow segment k and the edge junction point S_1 is designated to be c_k^e and the corresponding pressure and width values are designated as p_k^e and w_k^e respectively.

The flow rate out of the flow segment end S_2 can be similarly expressed as

$$q_{out}(w) = \frac{-w^3}{12\mu_f}\left[\frac{\hat{p}_2 - \hat{w}_2(K_n w - E_n)}{c_2 \hat{w}_2 + w^3}\right], \qquad (14)$$

with $\hat{p}_2$ and $\hat{w}_2$ defined by expressions analogous to Eq. (12) and Eq. (13) respectively and with the sum taken over the set of external flow segments J_2^e that are connected to the edge point S_2 (see Fig. 2).

Assembling the respective relationships for q_{in} and q_{out}, given by (11) and Eq. (14) respectively, the flow balance relationship Eq. (9) can be written as an implicit function of the flow width w in the form

$$G(w) = (q_{in} - q_{out} + Q_0)\Delta t + (c_1 + c_2)[w^p - w] = 0 . \qquad (15)$$

Since $G(w)$ is differentiable with respect to w, Eq. (15) is solved within each iterative cycle using Newton-Raphson iteration.

4. FLUID LAG FLOW BALANCE

In the case where the flow segment is partially filled with fluid, it is necessary to track the position of the fluid front. Let the fluid front distance from the flow segment edge S_1 be L as shown in Fig. 3. The fill fraction, φ, in the flow segment is therefore

$$\varphi = L/(c_1 + c_2). \tag{16}$$

The flow balance relationship corresponding to Eq. (9) that is obtained when the fluid front falls within the flow segment can now be written in the form

$$q_{in} = \frac{wL - w^p L^p}{\Delta t}, \tag{17}$$

where w^p and L^p are respectively the flow width and fluid front position in the previous time step, $t - \Delta t$. The flow rate into the partially filled segment is then assumed to be given by

$$q_{in} = \frac{-w^3}{12\mu_f}\left[\frac{-p^J}{L}\right]. \tag{18}$$

A suitably modified form of Eq. (15) must now be formulated to allow for the simultaneous solution of both the flow width w and the fluid front position, L. Applying Eq. (3) to the partially filled flow segment shown in Fig. 3, it can be seen that the dependence of the junction pressure on the partially filled segment width w and fluid front position L can be expressed as

$$p^J = \frac{\sum_{J_1^e} (w_k^e)^3 p_k^e / c_k^e}{(w^3/L) + \sum_{J_1^e} (w_k^e)^3 / c_k^e}. \tag{19}$$

The equivalent form for the average flow pressure, corresponding to Eq. (10) can be written as

$$K_n w - E_n = \frac{p^J L}{2(c_1 + c_2)}. \tag{20}$$

Substituting Eq. (19) into Eq. (20) provides a quadratic expression in L which can be solved to express L as an explicit function of w. This allows an appropriate flow balance function, analogous to Eq. (15), to be solved for w during each iterative evaluation of the flow balance for a partially filled flow segment.

The procedure described here has been implemented in a displacement discontinuity boundary element solution program called RIFT, [17]. The RIFT code allows for the incremental simulation of evolving fluid-driven fractures in plane strain. Fracture front propagation is controlled by specifying the crack tip asymptotic behaviour with zero fluid lag or with a fluid lag permitted. If a fluid lag is permitted, the propagating fracture is extended in incremental steps by introducing additional crack elements to selected crack tips in the element assembly. The local stress intensity is evaluated at each active crack tip at the end of each time step cycle. If the stress intensity exceeds the value of a specified mode I toughness value, K_{Ic}, an additional fracture element is appended to the crack tip in an appropriate growth direction. The growth direction is selected from a pre-defined mesh of candidate directions or is chosen to fall in the direction which corresponds to the maximum tensile "hoop" stress at a fixed distance ahead of the crack tip. (See, for example, [11, 12]). Consequently, the fracture front position is approximated to advance in a series of punctuated steps as the stress intensity at the edge element exceeds the assigned toughness value and then momentarily falls within each appended edge element. A more precise front tracking procedure has been described by Gordeliy and Detournay [10] where a variable time step procedure is implemented to solve for both the fluid front and crack front position.

An initial test of the behaviour of the junction pressure and partially filled fluid segment logic described here was carried out using the simple case of a single fracture with fluid injected at a central point. Two fracture fronts are propagated away from the injection point in a plane perpendicular the minimum principal field stress component. The flow parameters that were chosen are summarized in Table 1. Fig. 4 shows the evolving flow width profiles (connect lines with diamond markers) that arise after time intervals of 0.1 sec and 0.2 sec respectively. These results are compared to interpolated values obtained from the Oribi flow code described in [10]. It is apparent that there is very good agreement between the two procedures.

Fig. 5 shows a comparison between the width profile that is obtained when there is a zero lag at the crack tip and the flow follows a viscous-dominated crack tip opening width asymptote [2, 3, 14], to the case where the fluid front is tracked explicitly using the flow junction logic described in the present paper. (The remaining flow parameters are as shown in Table 1). A similar comparison is shown in Fig. 6 for the corresponding flow pressure profiles.

It is interesting to note from Fig. 5 that the crack edge in the case of the zero lag solution is in a similar position to the fluid front position in the analysis which allows a

development of the lag region. It would seem that the explicit simulation of the lag region could however have considerable significance in the case of flow network fluid injection simulations where pre-mobilization of discontinuities may be induced prior to the invasion of the fluid into the fractures. In addition, the assumption of the fluid lag can have an appreciable effect on the time history of the source point injection pressure, depending on the assumed values of the propagating fracture toughness. Fig. 7 compares the injection point fluid pressure for the crack propagation simulation with the fluid lag front explicitly tracked and the case where the fluid lag is assumed to be zero and the crack front asymptotic opening shape is assumed to be viscous controlled. Although the crack front toughness in both cases is implicitly "small" there is evidently a marked difference in the source pressure behaviour for the two cases. The fluctuations in the pressure-time profile shown in Fig. 7 can be ascribed to the stepped increase in the crack length as successive growth elements are appended to the crack tips.

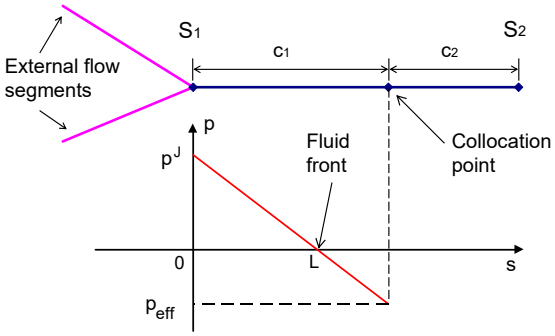

Fig. 3. Partially filled flow segment where the distance from the segment edge to the fluid front is L. The pressure is assumed to decrease linearly from p^J at the edge junction S_1 to zero at the front position.

Table 1. Fluid-driven fracture propagation test parameters.

Crack-normal field stress	10.0 MPa
Intact rock Young's modulus, E	72000 MPa
Intact rock Poisson's ratio, v	0.2
Fracture toughness, K_{Ic}	1.0 MPa.m$^{1/2}$
Fluid viscosity, μ_f	0.2 Pa.sec
Flow injection rate, Q_0	0.1 m^2/sec
Time step interval, Δt	0.0001 sec

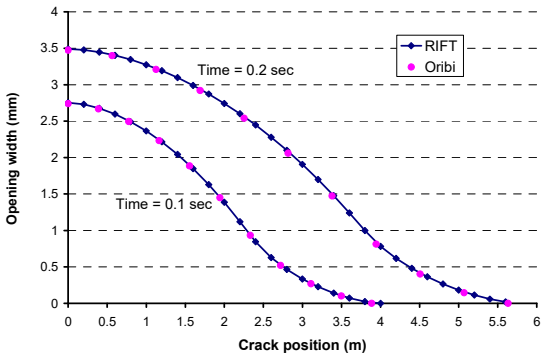

Fig. 4. Flow width profile comparison between flow code ORIBI (Gordeliy [10]) and the current algorithm implemented in RIFT.

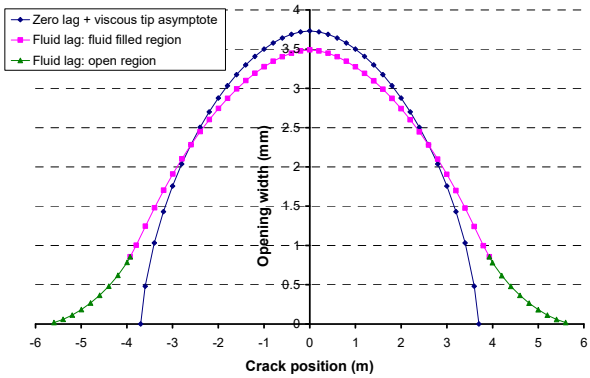

Fig. 5. Comparison of flow width profiles at time 0.2 sec for fractures propagated assuming, (a) a viscous-dominated crack tip asymptote with zero flow lag, (b) explicit fluid front tracking where the fluid front position is determined using a zero pressure condition at the front (the zero pressure lag region is explicitly marked).

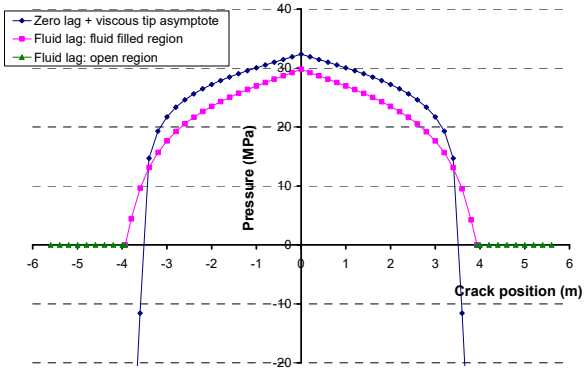

Fig. 6. Comparison of flow pressure profiles at time 0.2 sec for fractures propagated assuming, (a) a viscous-dominated crack tip asymptote with zero flow lag, (b) explicit fluid front tracking where the fluid front position is determined using a zero pressure condition at the front (the pressure is zero in the lag region).

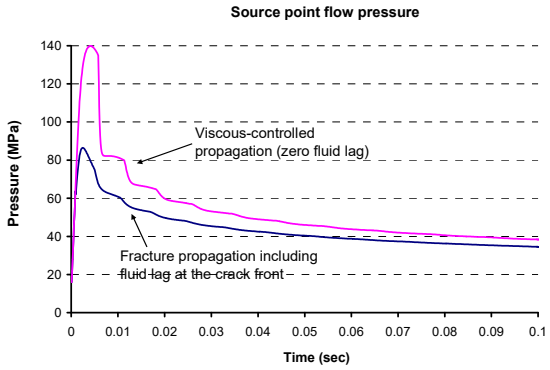

Fig. 7. Comparison of source flow pressure as a function of time for toughness-controlled fracture propagation, with the inclusion of a fluid lag region adjacent to the crack tip, and viscous-controlled propagation with zero fluid lag.

5. FLOW BRANCHING AND FLOW NETWORK SIMULATION

As an illustration of the flow branching logic developed in section 3, consider the case where flow is initiated at the central element of a straight flow path segment of length 2.2 m that is divided into 11 elements of length 0.2 m. The flow path is allowed to bifurcate into four branch segments at the ends of the initial segment. The separation angle between the branches at each end of the initial flow segment is 60 degrees. Plots of the evolved flow patterns at times t = 0.1 sec and t = 0.2 sec are shown in Fig. 8a and Fig. 8b respectively. It is interesting to note that the flow pattern is generally symmetric for the first plot at time 0.1 sec (Fig. 8a) but becomes somewhat asymmetrical at time 0.2 sec as indicated by the flow segments marked “Branch 1” and “Branch 2” in Fig. 8b.

Fig. 9 is a plot of the estimated average flow rate in the right-hand end element of the 2.2 m source flow segment, compared to the average flow rates in the initial elements of the Branch 1 and Branch 2 flow segments, shown in Fig. 8b. It is interesting to observe the progressive breaking of the flow rate symmetry between Branch 1 and Branch 2 in Fig. 9. It should be noted as well that the sum of the Branch 1 and Branch 2 flow rates shown in Fig. 9 do not imply a loss of fluid through the junction when compared to the average flow rate through the end element of the source segment. This apparent discrepancy arises because the average flow rates shown in Fig. 9 are computed for each element adjacent to the junction and not at the junction point itself. The overall fluid volume stored in the flow segments was found to be reasonably accurate and is over-estimated by approximately 1.0 percent at the simulation end time of t = 0.2 sec. (The total injected volume of fluid is 0.02 m^2 at this time).

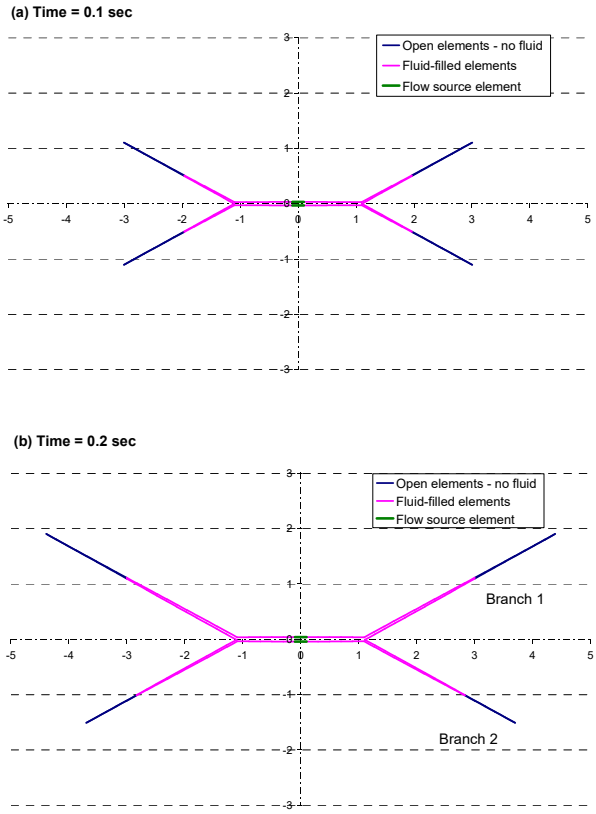

Fig. 8. Plot of fluid-filled and open crack elements in a constrained flow mesh with symmetrical flow branches at the ends of an initial flow segment. (a) Activated elements after elapsed time 0.1 sec. (b) Activated elements after elapsed time 0.2 sec.

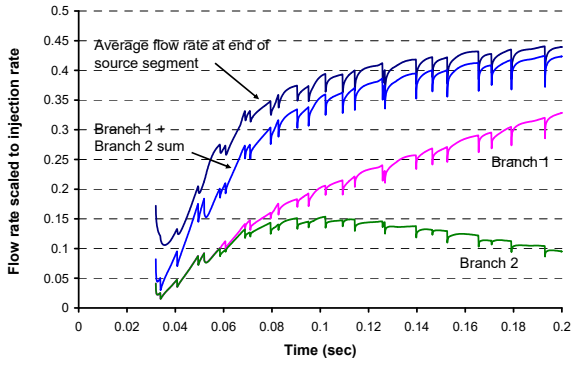

Fig. 9. Average flow rates at the last element of the source segment and at the initial elements in the right-hand flow branches shown in Fig. 8b. as a function of time. (The average element flow rates are scaled to the flow source injection rate).

A further illustration of the flow branching logic is given in Fig. 10 where fluid is allowed to propagate from one or two specified source elements in a random Delaunay flow path mesh. The flow is constrained to follow selected paths from the designated segments shown in Fig. 10. The maximum element length in the mesh is 0.3 m and each flow segment contains multiple flow elements. The primitive stress field is assumed to be hydrostatic and equal to 10 MPa. The flow source parameters correspond to the values given in Table 1.

The flow path selected for the case of a single flow injection element is shown in Fig. 11, indicating that a number of activated branch paths are terminated, subsequently leaving one major flow path that is confined to a relatively localised flow channel. A fairly extensive network of mobilized crack elements, which are not fluid filled, are seen to be joined to the ends of the fluid-filled segments.

Fig. 12 shows the results of repeating the simulation with two flow source elements. In this case, it can be seen that the lower flow path merges with the path that is propagated from source element 1 (See Fig. 10). Interestingly, relatively fewer unfilled but mobilized crack segments seem to be attached to the edges of the fluid-filled segments when compared to the fracture pattern shown in Fig. 11.

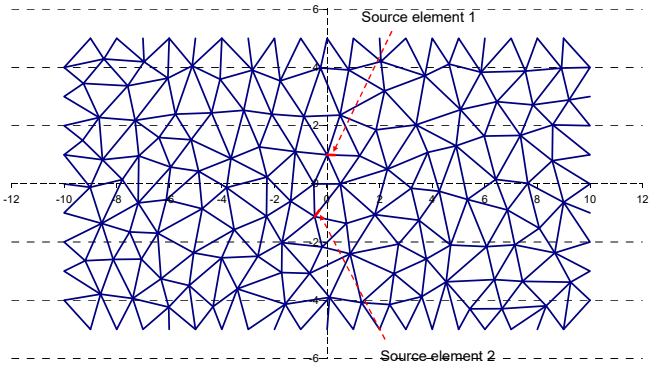

Fig. 10. Random Delaunay mesh flow network paths to illustrate flow branching evolution from one or two floe source injection elements. (Hydrostatic primitive stress field = 10 MPa).

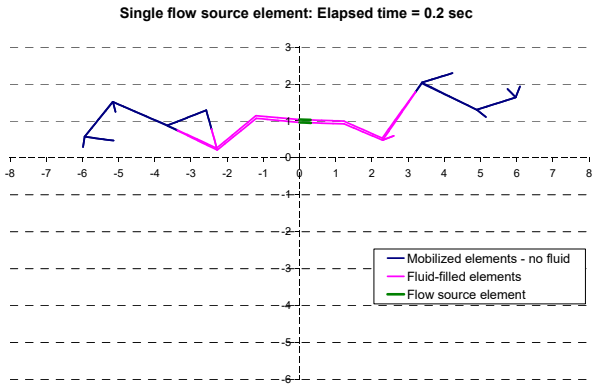

Fig. 11. Flow path evolution from flow source element 1 in the Delaunay mesh shown in Fig. 10. (Time = 0.2 sec).

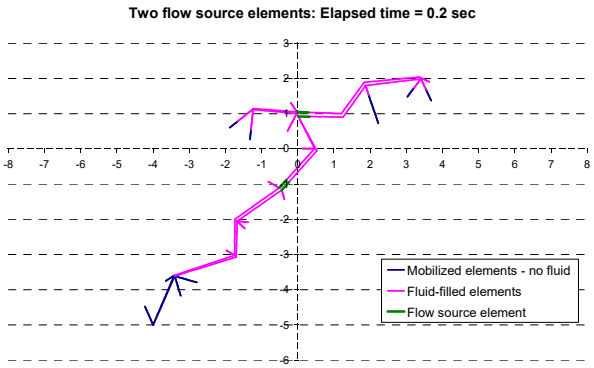

Fig. 12. Flow path evolution from both source elements 1 and 2 in the Delaunay mesh network shown in Fig. 10. (Time = 0.2 sec).

6. CONCLUSIONS

A simple procedure has been described to simulate flow path branching, including the ability to model the lag region between the fluid front and the mobilized fracture front. Preliminary results indicate that there is good agreement between the method developed in this paper and an independently developed approach that has been reported for tracking the fluid front position.

It appears that significant differences in the injection pressure-time history can arise between a flow propagation model that includes fluid lag with a nominal small toughness control for the crack tip advance and a propagation model with zero fluid lag and viscous-controlled asymptotic crack tip velocity. Simple applications of the model to flow branching simulations indicate as well that significant mobilization of non fluid-filled fractures may arise at the edges of fluid-filled fracture segments.

Future studies will attempt to extend the model developed here to the analysis of three-dimensional fluid-driven fractures.

ACKNOWLEDGEMENTS

We would like to acknowledge the assistance of Dr. Lisa Gordeliy in performing the cross-check numerical simulations of fluid lag.

REFERENCES

1. Spence, D.A. and P. Sharp. 1985. Self-similar solutions for elastohydrodynamic cavity flow. *Proc. R. Soc. Lond.* A. 400: 289-313.
2. Desroches, J., Detournay, E., Lenoach, B., Papanastasiou, P., Pearson, J.R.A., Thiercelin, M. and A. Cheng. 1994. The crack tip region in hydraulic fracturing. *Proc. R. Soc. Lond.* A. 447: 39-48.
3. Mitchell, S.L., Kuske, R. and A.P. Peirce. 2007. An asymptotic framework for the analysis of hydraulic fractures: The impermeable case. *Journal of Applied Mechanics*. 74: 365-372.
4. Detournay, E. 2004. Propagation regimes of fluid-driven fractures in impermeable rocks. *International Journal of Geomechanics*. 4: 35-45.
5. Garagash, D. and E. Detournay. 2000. The tip region of a fluid-driven fracture in an elastic medium. *Journal of Applied Mechanics*. 67: 183-192.
6. Garagash, D. 2006. Propagation of a plane-strain hydraulic fracture with a fluid lag: Early-time solution. The tip region of a fluid-driven fracture in an elastic medium. *Journal of Applied Mechanics*. 67: 183-192.
7. Lecampion, B. and E. Detournay. 2007. An implicit algorithm for the propagation of a hydraulic fracture with a fluid lag. *Comput. Methods Appl. Mech. Engrg*. 196: 4863-4880.
8. Carbonell, R., Desroches, J. and E. Detournay. 1999. A comparison between a semi-analytical and a numerical solution of a two-dimensional hydraulic fracture. *International Journal of Solids and Structures*. 36: 4869-4888.
9. Adachi, J., Siebrits, E., Peirce, A. and J. Desroches. 2007. Computer simulation of hydraulic fractures. *Int. J. Rock Mech. Min. Sci.* 44: 739-757.
10. Gordeliy, E. and E. Detournay. 2011. Displacement discontinuity method for modeling axisymmetric cracks in an elastic half-space. *International Journal of Solids and Structures*. 48: 2614-2629.
11. Zhang, X., Jeffrey, R.G. and M. Thiercelin. 2007. Deflection and propagation of fluid-driven fractures at frictional bedding interfaces: A numerical investigation. *Journal of Structural Geology*. 29: 396-410.
12. Zhang, X., Jeffrey, R.G. and M. Thiercelin. 2008. Escape of fluid-driven fractures from frictional bedding interfaces. *Journal of Structural Geology*. 30: 478-490.
13. Thiercelin, M. 2009. Hydraulic fracture propagation in discontinuous media. In *Proceedings of the International Conference on Rock Joints and Jointed Rock Masses*, Tucson, Arizona, USA.
14. Peirce, A. and E. Detournay. 2008. An implicit level set method for modeling hydraulically driven fractures. *Comput. Methods Appl. Mech. Engrg*. 197: 2858-2885.
15. Vallentine, H.S. *Applied Hydrodynamics*. Butterworth, 1969.
16. Crouch, S.L. and A.M. Starfield. 1983. *Boundary element methods in solid mechanics*. 1st ed. London: George Allen & Unwin.
17. Napier, J.A.L. and Malan, D.F. 2007. The computational analysis of shallow depth tabular mining problems, *J. S. Afr. Inst. Min. Metall.* 107: 725-742.
18. Lawn, B. 1993. *Fracture of brittle solids*, Cambridge University Press, 2nd Edition.